

1 **Vitamin E supplementation prevents ferroptosis in round spermatids of aged mice**

2

3

4 Jasper Germeraad, Takako Kikkawa, Noriko Osumi*

5

6 Department of Developmental Neuroscience, Tohoku University Graduate School of Medicine,
7 2-1, Seiryo-Machi, Aoba-ku, Sendai, Miyagi 980-8575, Japan

8

9 Running title: Ferroptotic cell death in the testes

10

11 Keywords: Spermatogenesis, cell death, ferroptosis

12

13 *Corresponding author

14 Noriko Osumi, PhD

15 Professor, Department of Developmental Neuroscience,

16 Tohoku University Graduate School of Medicine,

17 2-1 Seiryo-machi, Aoba-ku, Sendai 980-8575, Japan

18 Tel.: +81 22 717 8201. Fax: +81 22 717 8205.

19 E-mail address: noriko.osumi.c7@tohoku.ac.jp (N. Osumi)

20

21 Grant Sponsors: JSPS KAKENHI (#17K19372, 22K19322), The Canon Foundation

22 **Abstract**

23 Germ cell depletion in the aged testes has traditionally been attributed to removal by apoptosis.
24 This study aimed to determine whether ferroptosis, an alternative form of cell death driven by
25 iron-dependent lipid peroxidation, also contributes to germ cell loss in the lipid-rich
26 environment of the testis. Here, we demonstrate that pre-meiotic cells are eliminated via
27 apoptosis, whereas post-meiotic round spermatids (RSs) are mainly removed through
28 ferroptosis. Surprisingly, we detected a greater abundance of Y-chromosome-bearing RSs (Y-
29 RSs) than X-carrying RSs (X-RSs) in the aged testis, implying that X-RSs might be more prone
30 to ferroptosis. Young mice fed a vitamin E (VE) deficient diet recapitulated age-related
31 phenotypes, while VE supplementation prevented ferroptosis and promoted the survival of X-
32 RSs in aged mice. Overall, this study reveals that aging causes ferroptosis in RSs, specifically
33 impacting X-RSs, which can be prevented by VE supplementation, effectively reversing age-
34 induced deterioration and contributing to healthy testicular aging.

35 Introduction

36 In recent decades, a global demographic shift towards aging populations has resulted in delayed
37 marriages and parenthood^{1,2}, placing increasing pressure on healthcare systems. These trends
38 have contributed to higher risks of fertility challenges, pregnancy complications, and
39 neurodevelopmental disorders in offspring. While the reproductive lifespan of females is
40 biologically limited, male fertility, although maintained throughout life, experiences a gradual
41 decline with age³. Numerous studies have documented age-related reductions in semen volume,
42 sperm concentration and motility, as well as increased DNA fragmentation in sperm^{4,5,6}, which
43 collectively contribute to decreased reproductive potential. As a result, preserving male
44 reproductive health during aging has become increasingly important for couples seeking to
45 conceive later in life.

46 Sperm cells, produced through spermatogenesis, are essential for sexual reproduction, as they
47 carry either the X or Y chromosome, which determines the sex of the offspring.
48 Spermatogenesis occurs within the seminiferous tubules of the testis and takes approximately
49 75 days in humans and 35 days in mice⁷. The process starts with spermatogonial stem cells that
50 undergo asymmetric division to form spermatocytes. These spermatocytes then enter meiosis,
51 producing haploid round spermatids (RSs), which elongate and condense their genetic material,
52 ultimately developing into mature spermatozoa. While various studies have documented age-
53 related decline in murine spermatogenesis^{8,9,10}, the full implications of these changes on
54 reproductive health remain insufficiently understood.

55 Germ cell depletion is commonly described in the aged testis, typically attributed to apoptotic
56 elimination triggered by oxidative stress^{11,12}. However, we found a study reporting that
57 spermatocytes and RSs may respond differentially to oxidative stress, particularly to lipid
58 peroxides *in vitro*; while spermatocytes undergo apoptosis, RSs seem to die via ferroptosis¹³.
59 Ferroptosis is a regulated form of cell death, distinct from apoptosis, characterized by iron-
60 dependent oxidation of membrane phospholipids^{14,15} and the failure of Glutathione peroxidase
61 4 (Gpx4) to neutralize lipid peroxides¹⁶. Notably, Gpx4 was identified as indispensable for
62 preventing germ cell death already before the discovery of ferroptosis^{17,18}. These findings
63 suggest a previously undiscovered role of ferroptosis in the aging testis *in vivo*.

64 Vitamin E (VE), a group of fat-soluble micronutrients comprising of four tocopherols and four
65 tocotrienols, is well-known for its antioxidant properties and its ability to prevent ferroptosis
66 by inhibiting lipid peroxidation *in vitro*^{19,20}. VE has also been shown to positively impact the

67 male reproductive system and fertility across various species *in vivo*^{21,22}. Additionally, VE
68 deficiency (VED) has been reported in mice to cause alterations in the testis and epididymis
69 that closely resemble aging²³. These findings suggest a potential link between ferroptosis and
70 germ cell death during aging, which may be modulated by VE.

71 In this study, we demonstrate that premeiotic cells primarily undergo apoptosis, while RSs
72 predominantly initiate an alternative form of cell death, exhibiting key features of ferroptosis
73 as mice age. Surprisingly, we noticed an alteration in sex chromosome ratio among RSs of aged
74 mice, with a greater proportion of Y-chromosome bearing RSs (Y-RSs), likely due to increased
75 susceptibility of X-bearing RSs (X-RSs) to ferroptosis. Furthermore, VED was found to induce
76 ferroptosis and eventually alter the Y/X ratio, while VE supplementation reversed several
77 aging-related changes including improving RSs survival and restoring the YX ratio. Our
78 findings suggest that VE may hold clinical potential in mitigating aging-related testicular
79 decline by preserving RS viability.

80

81

82 Results

83 Round spermatids predominantly undergo a form of cell death distinct from apoptosis

84 We began by confirming aging-related phenotypic alterations in the testis of 18-month old mice.
85 As we expected, aged mice exhibited an increase in body weight (Fig. 1a) and a corresponding
86 decrease in testis weight (Fig. 1b), resulting in a lower gonadosomatic index²⁴ (testis
87 weight/body weight, GSI, Fig. 1c). Next, we assessed spermatogenesis within the seminiferous
88 tubules (Fig. 1d). In young mice, the tubules appeared morphologically intact, with a dense,
89 well-organized cell arrangement from the periphery to the lumen (Fig. 1e, upper panels). In
90 contrast, aged mice showed significant depletion of cells in both the peripheral and luminal
91 areas (Fig. 1e, lower panels). A detailed immunohistochemical germ cell analysis revealed a
92 marked reduction in the number of Type A spermatogonial cells (Type A Spg) in aged mice
93 compared to young mice (Fig. 1f), which extended to later stages of spermatogenesis, including
94 Type B spermatogonia (Type B Spg, Fig. 1g), meiotic pachytene spermatocytes (PSs, Fig. 1h),
95 and haploid RSs (Fig. 1i). Additionally, a decrease in the number of somatic Sertoli cells (SCs)
96 was observed in aged mice (Fig. 1j).

97 We next examined differential cell death mechanisms in young and aged testes by double
98 labeling with active caspase-3 (Casp3) and terminal deoxynucleotidyl transferase dUTP nick
99 end labelling (TUNEL). Casp3 is a marker specific for apoptosis, while TUNEL detects DNA

100 fragmentation associated with various forms of cell death, including ferroptosis²⁵. Our analysis
101 clearly showed a higher percentage of tubules containing TUNEL-positive (TUNEL+) cells in
102 aged mice compared to young mice (32% in young vs 46% in aged, Figure 2a). We then
103 calculated the cell death index (CDI), defined as the average number of dying cells per tubule
104 (TUNEL+ cells/tubule number). The CDI was significantly elevated in aged mice (Fig. 2b).

105 We further characterized cell death in pre-meiotic cells, including spermatogonia and PSs,
106 which are located in the peripheral region of the seminiferous tubules (between the dashed and
107 solid lines), and in post-meiotic RSs situated in the luminal area (inside the solid line) (Fig. 2c).
108 Cell death within the tubules exhibited heterogeneity; some tubules contained only
109 Casp3+/TUNEL+ cells, indicating apoptosis in the peripheral area (closed arrowheads, Fig. 2d,
110 d'), while others displayed a mixture of Casp3+/TUNEL+ apoptotic cells and Casp3-/TUNEL+
111 non-apoptotic cells (open arrowheads, Fig. 2e, e'). In other cases, only Casp3-/TUNEL+ cells
112 were observed in both the peripheral and luminal areas (Fig. 2f, f', g, g'). Interestingly, both
113 Casp3+/TUNEL+ and Casp3-/TUNEL+ cells were found in the peripheral area, but in the
114 luminal area, most dying cells were Casp3-/TUNEL+ (Fig. 2g, g'), with only few
115 Casp3+/TUNEL+ cells (Extended data 1).

116 We quantified these labeled cells in both regions of young and aged testes. In the aged testis,
117 there was a significant increase in Casp3+/TUNEL+ cells in the peripheral area compared to
118 the young testis (Fig. 2h), while the number of Casp3-/TUNEL+ cells remained unchanged
119 (Fig. 2h). In the luminal area, the number of Casp3+/TUNEL+ RSs was consistently low, with
120 no significant difference between age groups (Fig. 2i). However, aged mice showed a notable
121 increase in Casp3-/TUNEL+ RSs in aged mice (Fig. 2i). These findings suggest that aging
122 primarily induced apoptosis in pre-meiotic cells, whereas non-apoptotic cell death
123 predominated in post-meiotic RSs. This reveals a novel aspect of testicular degeneration due
124 to aging, highlighting a shift from apoptosis to non-apoptotic cell death in RSs.
125

126 **Round spermatids in aged mice exhibit hallmarks of ferroptosis**

127 We hypothesized that aging-related oxidative stress may trigger ferroptosis in RSs *in vivo*.
128 Therefore, we aimed to characterize ferroptosis in RSs at the molecular level by isolating RSs
129 from whole testes (Fig. 3a). Using a modified density gradient method²⁶, we collected fractions
130 that were microscopically assessed for round spermatid (RS) enrichment using PNA staining.
131 Fractions with >80% RSs purity were deemed sufficient for the following analyses (Fig. 3b).
132 With these RS-enriched fractions, we examined key molecular markers of ferroptosis. We

133 hypothesized that aging would result in a reduced levels of antioxidant enzyme Gpx4, along
134 with increased lipid peroxidation of polyunsaturated fatty acids (PUFAs) mediated by long-
135 chain-fatty-acid-CoA ligase 4 (*Acsl4*), and arachidonate 15-lipoxygenase (*Alox15*) (Fig. 3c).

136 We first histologically confirmed the expression of Gpx4 in the cytoplasm of RSs and in the
137 tail region of sperm, while weak expression was observed in spermatocytes. However, no
138 obvious difference between young and aged testes was observed (Fig. 3d). Gpx4 exists in three
139 isoforms: nuclear (nGpx4), mitochondrial (mGpx4), and cytosolic (cGpx4). Previous studies
140 have reported that while both nGpx4 and mGpx4 are indispensable for spermatogenesis, cGpx4
141 plays a crucial role in protecting germ cells from cell death^{17,27}. We therefore sought to
142 determine which isoforms are affected by aging. Western blot analysis using an anti-Gpx4
143 antibody that recognizes both mGpx4 and cGpx4 isoforms, revealed no significant difference
144 in Gpx4 protein levels (approximately 17 kDa) between young and aged RS-enriched fractions
145 (Fig. 3e). To further assess isoform-specific expression at the mRNA level, we conducted
146 quantitative PCR (qPCR). In aged RSs, we found that the expression levels of both *nGpx4* and
147 *mGpx4* remained unchanged (Fig. 3f, g). However, *cGpx4* expression was significantly reduced
148 in aged RSs (Fig. 3h).

149 Next we examined lipid peroxidation in RSs. Quantification of *Acsl4* and *Alox15* expression in
150 RS-enriched fractions from young and aged testes revealed a significant increase in aged RSs
151 (Fig. 3i, j). Since *Acsl4* and *Alox15* promote PUFA oxidation, leading to the production of
152 aldehydes like 4-Hydroxynonenal (4HNE), a key marker of lipid peroxidation, we quantified
153 4HNE levels by Western blot analysis. This revealed a significant increase in the 4HNE levels
154 in RS-enriched fractions from the aged testes (Fig. 3k). These findings indicate that aged RSs
155 accumulate lipid peroxides, as evidenced by the upregulation of *Acsl4* and *Alox15*, along with
156 increased 4HNE levels. The concurrent reduction in *cGpx4* expression suggests a diminished
157 capacity to neutralize reactive oxygen species (ROS), which may promote ferroptosis as a
158 distinct cell death pathway in RSs, contrasting to the apoptotic mechanism observed in
159 spermatogonia and spermatocytes.

160 We then investigated potential differences in cell death vulnerability between X-RSs and Y-
161 RSs. During spermatogenesis, X-RSs and Y-RSs are theoretically produced in equal proportions
162 through meiosis. However, using fluorescent *in situ* hybridization (FISH), we unexpectedly
163 discovered that the sex chromosome ratio in the aged testis was skewed towards Y-RSs
164 compared to the young testis (young: 1.02 vs aged: 1.11; $P < 0.001$, Fig. 3l). This finding
165 suggests that aging may selectively impact the survival of X-RSs. Given the established

166 relationship between reduced *cGpx4* levels, lipid peroxidation and ferroptosis, it is plausible
167 that X-RSs are more susceptible to ferroptosis. This increased vulnerability could lead to the
168 observed skewed Y/X ratio in the aged testis.

169

170 **Vitamin E ensures RSs survival and restores the Y/X ratio alteration**

171 Given the observed susceptibility of RSs to oxidative stress and ferroptosis, we next
172 investigated whether varying dietary levels of VE, a potent antioxidant, could mitigate these
173 age-related changes in RS survival and restore the skewed Y/X ratio. To simulate the effect of
174 aging, we fed young mice either a control diet (YC) or VE-deficient diet (YVE-), while to
175 counteract aging effects, we provided aged mice either a control diet (AC) or VE-supplemented
176 diet (AVE+) (Fig. 4a).

177 We first assessed whether VE- or VE+ diets would result in systemic health abnormalities by
178 measuring bodyweight. While body weight naturally increased over time across all groups, it
179 remained unaffected by dietary changes (Extended Data Fig. 2a, b). Similarly, testis weight
180 and GSI showed no significant alterations under these dietary conditions (Extended Data Fig.
181 2c, d). However, the progression of spermatogenesis was influenced by VE modulation (Fig.
182 4b, Extended Data Fig. 2e). Cell-count analyses revealed an age-related decline in Type A and
183 B Spg in both AC and AVE+ groups (Extended Data Fig. 2f, g). PSs showed a moderate
184 sensitivity to VE levels, exhibiting a slight but non-significant decrease in the YVE- group and
185 a minor increase in the AVE+ group (Extended Data Fig. 2h). In contrast, RSs were highly
186 responsive to VE modulation, demonstrating significant reductions in the YVE- group and,
187 conversely, partial recovery in the AVE+ group (Fig. 4b, c). These findings suggest that VE
188 plays a crucial role in modulating spermatogenesis, particularly by mitigating age-related
189 declines in RSs and enhancing their recovery under VE+ conditions.

190 Analyzing cell death under the influence of VE (Fig. 4d, Extended Data Fig. i), we found that
191 the testes of YVE- and AC mice had the highest percentage of tubules containing TUNEL+
192 cells, while the percentage was reduced in AVE+ mice (YC: 28%, YVE-: 40%, AC: 41%,
193 AVE: 30%, Fig. 4e). Similar trends were observed for the CDI (Fig. 4f). In the peripheral region
194 of the testis, neither VE- nor VE+ significantly affected the number of Casp3+/TUNEL+ cells
195 (Fig. 4g) or Casp3-/TUNEL+ cells (Extended Data Fig. 2i, j). However, in the lumen, RSs were
196 notably impacted; YVE- led an increase in Casp3-/TUNEL+ RSs, while AVE+ reduced the
197 number of these cells (Fig. 4h). Casp3+/TUNEL+ RSs remained rare and unchanged across all
198 groups (Extended Data Fig. 2i, k). These observations imply that while VE modulation has

199 minimal effects on apoptosis in peripheral testis cells, it significantly influences RS survival,
200 with VE- increasing and VE+ reducing cell death.

201 We next assessed whether VE modulation affected the molecular hallmarks of ferroptosis in
202 RSs. No significant changes were observed in Gpx4 protein levels across the groups (Fig. 4i)
203 nor in mRNA levels for *nGpx4*, or *mGpx4* (Fig. 4j, k). However, *cGpx4*, showed a slight, yet
204 non-significant reduction in YVE- group, while no changes in *cGpx4* mRNA levels were
205 observed in AVE+ compared to AC (Fig. 4l). In terms of lipid peroxidation markers, there was
206 a marginal, but non-significant, increase in *Acsl4* mRNA levels in YVE-, with no changes
207 observed in AVE+ (Fig. 4m). *Alox15* expression remained unaffected in both YVE- and AVE+
208 groups (Fig. 4n). Notably, however, 4HNE levels were significantly altered; they were elevated
209 in YVE- group and dramatically reduced in AVE+ compared with AC (Fig. 4o). These results
210 indicate that while VE modulation does not significantly affect a key ferroptosis-related
211 enzyme like Gpx4, it has a pronounced impact on lipid peroxidation, as evidenced by the
212 marked changes in 4HNE levels, suggesting a protective role of VE against oxidative damage
213 in RSs.

214 Lastly, we evaluated the effect of VE on the Y/X ratio. As expected, the Y chromosome became
215 more dominant in the RSs of the YVE- group (YC: 1.02 vs YVE-: 1.07; $P=0.023$). On the
216 contrary, the AVE+ group show a marked decrease in the Y/X ratio compared to AC, resulting
217 in a ratio similar to the young control condition (AC: 1.10 vs AVE+: 1.01, $P=<0.001$, Fig. 4p).
218 Taken together, these data suggest that VE- accelerates testicular aging, as evidenced by
219 increased cell death, oxidative stress, and Y-chromosome dominance, while VE+ in aged mice
220 partially reversed these aging effects by improving RS survival, reducing lipid peroxidation,
221 and restoring the Y/X ratio, potentially by lowering the risk of ferroptosis in X-RSs.

222

223

224 Discussion

225 In humans, aging is associated with significant changes in the testes, including reductions in
226 testicular volume and weight^{28,29}. Similar aging effects have been reported in rodent models by
227 us and others^{10,30}. The observed reduction in testicular weight is largely attributed to the loss
228 of both germ cells and Sertoli cells, resulting from impaired spermatogenesis^{31,32,33}. In
229 aged mice, we observed a decline in the number of Type A Spg and Type B Spg, PSs, RSs, and
230 SCs, all of which likely contribute to the noted loss in testicular weight.

231 In this study, we focused on aging-induced cell death during spermatogenesis. Previous studies
232 have identified aging-related apoptosis in the murine testis^{34,35}, consistent with findings in
233 other tissues^{36,37}. Our analysis of young and aged testes revealed that different germ cell types
234 initiate distinct forms of cell death. Specifically, our results suggest that pre-meiotic male germ
235 cells predominantly undergo apoptosis, whereas post-meiotic RSs display a preference for
236 ferroptosis. This distinction aligns with findings from a previous *in vitro* study¹³. Furthermore,
237 research from our laboratory, investigating miRNA expression in sperm from aged mice, has
238 revealed a significant upregulation of miRNAs that target both apoptosis and ferroptosis³⁸. This
239 suggests that cells at different stages of development possess the necessary machinery to initiate
240 distinct cell death pathways in response to alterations in the aging testicular environment.

241 A previous ultrastructural and histological study using electron microscopy, toluidine blue and
242 acridine orange (dyes to label different types of cell death), has suggested that RSs rarely initiate
243 apoptosis in normal, healthy testes³⁹. In our study, we observed many RSs positive for TUNEL
244 but negative for Casp3. This suggests that RSs in aged mice appear to favor a non-apoptotic
245 cell death pathway. We indeed identified a combination of molecular hallmarks of ferroptosis
246 in RSs of aged mice, indicating that this might be the predominant cell death modality in these
247 cells. Specifically, we observed increased mRNA levels of *Acsl4* and *Alox15*, along with
248 reduced *cGpx4*, leading to elevated lipid peroxidation, as evidenced by higher 4HNE levels.
249 These lines of evidence collectively align with the characteristics of ferroptosis observed in
250 somatic cell lines^{16,40}, implying that aging may sensitize RSs to this form of cell death. This
251 heightened vulnerability may be partly explained by an increased incorporation of arachidonic
252 acid-derived PUFAs into membranes of RSs compared to other germ cells⁴¹, making them
253 more susceptible to aging-related oxidative stress.

254 Mammalian Y-chromosomes are essential for sex determination in offspring and are expected
255 to be present in a 1:1 ratio to X-chromosomes in haploid RSs. Surprisingly, we detected a
256 higher number of Y chromosomes than X chromosomes in the aged RS population, shifting
257 the ratio (young: Y/X 1:02, $n=13,303$, $N=6$ vs aged: Y/X: 1.11, $n=13,008$, $N=6$). To our
258 knowledge, this is the first study that investigated the skewed sex chromosome ratio in aged
259 RSs. A previous study examined the Y/X ratio in RSs in young (8-week old) mice and found
260 no difference between Y and X chromosome numbers (Y/X: 1.02, $n=2,029$)⁴², which aligns
261 with our observations in young (12-week old) mice. Other studies have focused on the Y/X
262 ratio of mature sperm in healthy men, with mixed results: some reported an excess of X
263 chromosomes⁴³, others found no difference⁴⁴, while another observed a predominance of Y

264 chromosomes⁴⁵. Whether the aging-altered Y/X ratio in RSs persists in mature sperm remains
265 to be investigated.

266 We present compelling evidence that X-RSs are more vulnerable to aging-related
267 environmental changes than Y-RSs, suggesting that X-RSs may selectively be eliminated. The
268 reason why X-RSs preferentially die, potentially via ferroptosis, remains unclear. One possible
269 explanation is that X-RSs are more susceptible to lipid peroxidation because *Acsl4*, which we
270 found to be upregulated in aged RSs, is located on the X chromosome⁴⁶. In addition, during
271 spermatogenesis, round spermatids remain physically bound through cytoplasmic bridges,
272 facilitating the sharing of gene products to maintain transcriptional diploidy. However, some
273 gene transcripts have been observed to not be equally shared, suggesting the potential for allelic
274 bias in gene expression⁴⁷. Upon reanalyzing their data⁴⁷, we found that several genes involved
275 in ferroptosis, including *Lpcat3* and *Dhr7*, are only partially shared, with an allelic bias
276 favoring X-RSs. These findings imply that lipid peroxidation levels might naturally be higher
277 in X-RSs, and with the age-related reduction of *Gpx4*, X-RSs might be more susceptible to
278 ferroptosis in response to oxidative stress.

279 Our observations in VE- recapitulated the characteristics of aged testes, a finding consistent
280 with a previous report that studied the influence of VE- in mice testes at the morphological
281 level²³. In contrast, VE+ mice showed partial restoration of certain aging parameters,
282 suggesting that lipid-related oxidative stress may play a key role in modulating aging-related
283 changes. Specifically, our findings suggest that VE modulation primarily affects RSs, as shown
284 by changes in their cell number in both VE- and VE+ groups, while other cell types were
285 largely unaffected. In line, a previous study showed that rats fed VE- diet from postnatal day
286 10 (P10) and sacrificed at P42 (before completion of the first spermatogenic wave), halted
287 spermatogenesis at the RS stage, while other germ cells remained present⁴⁸. We observed that
288 spermatogenesis continued beyond the RS stage, likely because our VE dietary intervention
289 was initiated in sexually mature mice and the feeding period (10 weeks, covering two cycles
290 of spermatogenesis) was not sufficient to induce complete arrest. Nonetheless, these lines of
291 evidence underscore the critical role of VE in survival of RSs.

292 We found that VE modulation may influence the initiation of ferroptosis independently of
293 *cGpx4*, *Acsl4* and *Alox15* function, as evidenced by its impact on 4HNE levels in both VED
294 and VE+ conditions. Other studies have shown that *Gpx4* and VE cooperatively protect
295 regulatory T cells and hematopoietic stem cells from ferroptosis^{49,50}, suggesting that interaction
296 between *Gpx4* and VE may be cell-type or tissue-specific. Regarding the vulnerability of

297 ferroptosis in RSs, VE plays a critical role in supporting the survival of RSs, particularly X-
298 RSs, by preventing the initiation of ferroptosis through neutralization of lipid peroxy radicals
299 in aged mice.

300 Overall, our data suggest that VE supplementation may help prevent aging-related changes in
301 the testis, with notable benefits for RSs. It is reported that VE supplementation can potentially
302 enhance the success of a *in vitro* fertilization technique by injecting RSs for men with complete
303 meiotic arrest⁵¹. Furthermore, it has recently been reported that overall sperm count worldwide
304 decreased in men from 1973 to 2018, even after accounting for confounders, including age^{52,53}.
305 As such, VE supplementation might be beneficial not only for aged men but also for young
306 men. However, our study has a few limitations. We do not present direct evidence that
307 ferroptosis induces the skewed Y/X ratio in RSs, nor do we have data on the long-term effects
308 of VE supplementation in clinical applications, including optimal concentrations or ideal
309 delivery methods. Additionally, it remains unclear whether the altered Y/X ratio persists in
310 mature sperm or if VE supplementation can influence live birth ratios in aged mice. These
311 questions merit further investigation.

312 **Methods**
313 **Animals**
314 C57BL/6J mice were obtained from Charles River laboratories and were bred and maintained
315 in the Animal Experiment Facility at the Tohoku University Graduate School of Medicine.
316 Mice were sacrificed at 3 months old (Young) or 18 months old (Aged). All animals were
317 housed in standard cages in a temperature- and humidity-controlled room on a 12-hour
318 light/dark cycle (light on at 8 am) and had access to food and water *ad libitum*. All experimental
319 procedures were approved by the Ethics Committee for Animal Experiments in Tohoku
320 University (#2023-MED03701) and the animals were treated according to the National
321 Institutes of Health (NIH) guide for the care and use of laboratory animals.

322

323 **Testis collection**

324 Animals were sacrificed by short sedation with isoflurane (MSD Animal health) and cervical
325 dislocation. Testes were isolated from the peritoneal cavity and separated from the surrounding
326 fat tissue and epididymis. Testis samples were fixed in 4% paraformaldehyde in phosphate
327 buffered saline (PBS, 4% PFA, Nacalai-Tesque) for 2 hours at 4°C, cut in half, and fixed for
328 an additional 18 hours. Cryopreservation was executed as follows: the testes samples were
329 immersed, sequentially, in 10% sucrose dissolved in PBS for 1 hour and 20% sucrose in PBS
330 overnight, both at 4°C. After cryopreservation, samples were frozen in Tissue-Tek optimal
331 cutting compound (OCT, Sakura Finetek) on a metal pedestal using liquid nitrogen and stored
332 in -80°C until further use. Cryosections (10µm) were obtained using a cryostat (Leica CM3050
333 S) and used for histological analyses.

334

335 **Immunohistochemistry (IHC)**

336 Testicular sections on slide glasses (Matsunami) were immunostained using antibodies
337 targeting anti-Plzf (1:500, sc28319, Santa Cruz), anti-Scp3 (1:500, ab97672, Abcam), anti-Kit
338 (1:500, D13A2, Cell Signalling technologies), anti-Sox9 (1:900, 5535, EMD Millipore), and
339 anti-Gpx4 (1:1000, ab125066, Abcam). Sections were washed using Tris-buffered saline
340 containing 0.1% Tween20 (TBST). Antigen retrieval was performed (except for anti-cKit), for
341 10 minutes in 0.01 M citrate buffer (pH 6.0) at 95°C. Afterwards, slides were washed 3 times
342 for 10 min-each with TBST, and subsequently blocked with 3% Bovine serum albumin (BSA)
343 and 0.3% Triton X-100 in PBS for 1 hour at room temperature (RT). The slides were then
344 incubated with primary antibodies diluted in blocking solution overnight at 4°C, washed again
345 with TBST and incubated for 1 hour at RT with 4', 6-diamino-2-phenylindole (DAPI, 1:1000,

346 Sigma) as well as secondary antibodies (1:500, Anti-mouse alexa 488 or anti-rabbit Cy3,
347 Jackson ImmunoResearch) or peanut agglutinin (PNA-Cy5, 1:2000, Vector Laboratories)
348 when staining the acrosome for round spermatid identification. The sections were washed again
349 with TBST and mounted with Prolong Glass Antifade Mountant (Thermofisher). All images
350 were obtained using a confocal laser-scanning microscope (LSM800, Carl Zeiss), and
351 subsequently processed in Fiji (ImageJ).

352

353 **Fluorescent *in situ* hybridization**

354 FISH was performed as described previously⁵⁴. In short, slides with frozen sections of the testis
355 were subjected to antigen retrieval in Histo-VT One (Nacalai-Tesque) for 30 minutes at 90°C
356 and denatured using 50% formamid/2x saline-sodium citrate buffer (SSC), followed by
357 dehydration using 70% and 100% ethanol. A custom mixture of X (Conjugated with Cy3) and
358 Y (conjugated with FITC) chromosome probes (Chromosome Science Labo) was applied
359 subsequently. The slides were covered with hybridization cover (Hybrislip, Thermofisher) and
360 incubated at 80°C for 10 minutes. Hybridization occurred overnight in a humid chamber at
361 37°C. IHC was performed to enhance probe signals. Blocking was performed using 5%
362 Blocking One solution (Nacalai-Tesque) for 1 hour at RT. Primary antibodies (anti-FITC,
363 1:2000, A889, Invitrogen and Anti-Cy3, 1:2000, sc-166894, Santa Cruz) were diluted in 5%
364 Blocking One solution and incubated 1 hour at RT. After washing with 4x SSC, secondary
365 antibodies (1:2000, Anti-rabbit alexa 488 and anti-mouse Cy3, Jackson ImmunoResearch)
366 together with HOECHST-44432 (1:5000, Thermofisher) were applied and incubated for 1 hour
367 at RT. Slides were mounted with Prolong Glass Antifade Mountant (Thermofisher).. All
368 images were obtained using a fluorescence microscope (Keyence BZ-X series) and processed
369 in Fiji. RSs were identified according to nuclear morphology and location within the tubule.
370 Hybridridization efficiency was determined by microscopic evaluation and images were deemed
371 appropriate for analysis when in more than 95% of cells, a sex chromosome could be assigned.

372

373 **Cell death detection**

374 Apoptotic or non-apoptotic cell death was identified by double labeling for terminal
375 deoxynucleotidyl transferase dUTP nick end labelling (TUNEL, Merck Millipore) and
376 subsequently for an antibody against active-caspase-3 (1:500, 559565, BD Biosciences).
377 TUNEL labeling was performed first and according to the manufacturers' instructions. In short,
378 slides with testis sections were washed 1x 5 min in PBS and subjected to antigen retrieval by
379 microwaving 5 minutes in 0.01M citrate buffer. TdT mixture was applied and incubated at

37°C for one hour followed by incubation with an anti-digoxigenin antibody conjugated with fluorescein at RT for 30 min. Next, active-caspase-3 IHC was performed. Slides with testicular sections were covered in blocking solution (3% BSA and 0.3% Triton X-100 in PBS) at RT for one hour followed by primary antibody incubation at RT for one hour. Slides were washed three times for five min in PBS and incubated with a secondary antibody (1:500, Anti-rabbit-Cy3, Jacksonimmunoresearch) and HOECHST-44432 (1:5000) for one hour at RT. The slides were washed again in PBS and mounted with Prolong Glass Antifade Mountant (Thermofisher). and finally analysed with a confocal laser-scanning microscope (LSM800, Carl Zeiss). Using Fiji, male germ line cells in the periphery or in the region towards the lumen of the seminiferous tissue were independently quantified.

390

391 **Round spermatid isolation**

392 Round spermatid isolation was performed according to a previously published method²⁶. Briefly, fresh testicular tissue was harvested from young or aged male mice followed by removal of the epididymis and tunica albuginea. A single cell suspension was obtained via serial digestion with Collagenase IV (1mg/ml, Sigma) and Trypsin (0.6 mg/ml, Worthington) / DNase I (>3.2 ku/ml, Sigma) dissolved in 1x Krebs bicarbonate buffer (containing 1.2 mM KH₂PO₄, 0.35 mM MgSO₄, 1.7 mM CaCl₂, 4.7 mM KCl & 2.5 mM NaHCO₃) . The cell suspension was loaded on a 1-5% BSA / Krebs buffer gradient and allowed to sediment for 1.5 hour on ice at 1 unit gravity. Twenty-eight fractions of 1 mL were collected and analysed for purity using PNA (1:2000, Rhodamine, Vector Laboratories) and DAPI (1:1000, Sigma). Only fractions #4-7 were routinely enriched with RSs (>80%). Therefore, in subsequent isolations, fractions #4-7 were collected and pooled. The fractions were washed with Krebs buffer to remove excess BSA and immediately used for RNA and protein isolation.

404

405 **Simultaneous RNA and Protein isolation**

406 The simultaneous isolation of RNA and Protein was carried out using the AllPrep DNA/RNA/Protein mini kit (Qiagen) according to the manufacturers protocol with minor 407 modifications. All reagents and spin columns are supplied by the AllPrep mini kit (except for 408 Sodium dodecyl sulfate (SDS) buffer). In short, tissue was lysed in RLT buffer containing 1% 409 β-mercapto-ethanol (Sigma). The lysate was applied to the DNA spin column to remove DNA. 410 The flow-through was subsequently mixed with 100% ethanol and transferred to the RNA 411 binding column spin column. After centrifugation, flow-through was kept aside for protein 412 binding.

413 isolation while RNA was bound to the column. The column was subjected to washes with RW1
414 and RPE buffers, after which RNA was eluted using RNase free water and assessed for
415 concentration and purity using the Nanodrop (Thermofisher). Isolated RNA was stored at -
416 80°C until further used for complementary DNA (cDNA) synthesis. To the flow-through
417 containing protein, buffer APP was added and incubated for 10 minutes at RT. The sample was
418 pelleted, and 70% ethanol was added. The pellet was air dried and then vortexed for 1 minute
419 in SDS buffer containing 4% SDS, 20% sucrose, 10 mM Tris-HCL pH 6.8 and 1x
420 ethylenediaminetetraacetic acid (EDTA) free protease inhibitor (Roche) followed by
421 incubation at 37°C for 30 minutes. The protein sample was vortexed for 5 minutes and was
422 next pelleted via centrifugation. Supernatant was transferred to a new tube and protein
423 concentration was determined using the bicinchoninic acid assay (BCA, Nacalai-Tesque).
424 Protein samples were stored in -80°C until used for western blot.

425

426 **cDNA synthesis and quantitative polymerase chain reaction (qPCR)**

427 RNA isolated from pooled round spermatid fractions (1µg) was reverse transcribed into
428 cDNA using the SuperScript III™ First-Strand Synthesis System for RT-PCR (18080-400,
429 Invitrogen). cDNA was subsequently used for qPCR using Taq Pro Universal SYBR qPCR
430 Master Mix (Vazyme). Primer sequences used in this study can be found in Supplementary
431 Table 1. For *Gpx4*, 3 primer sets were used to quantify the isoforms with a set targeting
432 *nGpx4* and *mGpx4* individually and a set that targeted both *mGpx4* and *cGpx4*. Cytosolic
433 *Gpx4* was quantified by subtracting *Act* values of mitochondrial *Gpx4* from cytosolic +
434 mitochondrial *Gpx4*. All Values were normalized against *ActB* as a reference gene using the
435 $2^{-\Delta\Delta ct}$ method.

436

437 **Western blot**

438 Protein samples (5 µg) were separated by SDS-PAGE at 150V for 50 minutes (12%, TGX™
439 FastCast™ Acrylamide Kit; Bio-Rad). Primary antibodies targeting Gpx4 (1:1000, ab125066,
440 Abcam), 4-hydroxynonenal (4HNE, 1:1000, ab46545, Abcam), ActB (1:2500, sc-47778, Santa
441 Cruz), and Gapdh (1:4000, ab8245, Abcam) were used. Proteins were transferred onto 0.2 µm
442 polyvinylidene difluoride membranes (PDVF) via turboblot transfer (Trans-Blot Turbo Mini
443 PVDF Transfer Packs, Bio-rad), at 2.5A, 25V, 3 min. The membranes were then blocked in
444 10% Li-cor Intercept TBS blocking buffer (Licor) for 1 hour (Gpx4 & ActB) or in 5% blocking
445 One (Nacalai-Tesque) for 30 min (4HNE & Gapdh), and incubated with primary antibodies

446 overnight at 4 °C. The membrane was washed with Tris-buffered saline with 0.1% Tween-20
447 (TBST) and incubated with a secondary antibody (Gpx4 1:10000 or 4HNE 1:10000, W4011,
448 Promega and Gapdh 1:10000 or ActB 1:5000, W4021, Promega), diluted in 10% TBS blocking
449 buffer (Licor) or 5% blocking One (Nacalai-Tesque) for 1 hour at RT. The membranes were
450 then washed with TBST and visualized using the Bio-rad ChemiDoc Touch Gel Imaging
451 system and quantified relative to ActB for Gpx4 and Gapdh for 4HNE using Fiji.
452

453 **Vitamin E feeding**

454 For this experiment, young and aged C57BL/6J mice were purchased from Jackson laboratories
455 (JAX, Japan) as age-matched mice were available at the time of purchase. Differences in
456 bodyweight and testis were assessed and accounted for. Diets were custom-made and ordered
457 from Funabashi Farm, Japan. Young mice were fed control (containing 135 mg/kg VE), or
458 vitamin E deficient diet (containing >0.1 mg/kg VE). Aged mice were maintained on control,
459 VE-, or VE+ diet (containing 500 mg/kg VE). Detailed ingredients are listed in Supplementary
460 Table 2. All mice were raised on these diets for 10 weeks (70 days), covering two full cycles
461 of spermatogenesis (35 days)⁷. Young and aged mice were sacrificed at three and 18 months
462 of age, respectively. Testes were extracted as described with minor modifications: one testis
463 was cut in half, and one half was fixed using 4% PFA, cryopreserved and sectioned (10µm)
464 using a Leica 3050S cryostat as described previously. RSs were isolated from the remaining
465 testicular tissue (one and a half), after which RNA and protein were isolated simultaneously
466 from RS fractions. Testicular sections and RNA/protein were prepared for histology, qPCR
467 and Western blot experiments as described above.
468

469 **Statistical analysis**

470 Statistical information for individual experiments is shown in corresponding figure legends.
471 Values are always presented as mean± standard deviation. Data were first analysed for
472 normality by Shapiro-wilk test. Statistical comparisons between groups were then analysed for
473 significance by Student's *t*-test, Mann-Whitney U test, One-way ANOVA, followed by
474 Tukey's multiple corrections, Kruskal-Wallis test followed by Dunn's multiple corrections, or
475 Mixed-Model (Fixed effects: diet, week and bodyweight, Random effects: individual mice,
476 using repeated measures). Results were considered significant at *P*<0.05. Statistical analyses
477 were conducted using GraphPad Prism 10 (GraphPad Software).

478
479

480 **Declaration of interest**

481 The authors declare no conflict of interest.

482

483

484 **Acknowledgements**

485 We are grateful for the financial support from Japanese Society for the Promotion of Science
486 Kakenhi grant number #17K19372 and #22K19322, The Canon Foundation awarded to N.O,
487 and The establishment of university fellowships towards the creation of science technology
488 innovation, grant number JPMJFS2102, JPMJSP2114 awarded to J.G. We thank Ms. Sayaka
489 Makino for animal care and all other members of the Developmental Neuroscience laboratory
490 at Tohoku University for their useful comments.

491

492

493 **Author contributions**

494 Study design: J.G, TK, N.O; Data collection: J.G, T.K ; Data analysis: J.G; Drafted the
495 manuscript: J.G; Edited the manuscript: N.O, T.K; Funding acquisition: N.O, J.G.

496

497

- 498 **References**
- 499 1. Raymo, J. M. The second demographic transition in Japan: a review of the evidence.
500 *China Popul Dev Stud* **6**, 267–287 (2022).
- 501 2. Schmidt, L., Sobotka, T., Bentzen, J. G. & Nyboe Andersen, A. Demographic and
502 medical consequences of the postponement of parenthood. *Hum Reprod Update* **18**,
503 29–43 (2012).
- 504 3. Martins da Silva, S. & Anderson, R. A. Reproductive axis ageing and fertility in men.
505 *Rev Endocr Metab Disord* **23**, 1109–1121 (2022).
- 506 4. Johnson, S. L., Dunleavy, J., Gemmell, N. J. & Nakagawa, S. Consistent age-dependent
507 declines in human semen quality: A systematic review and meta-analysis. *Ageing Res
508 Rev* **19**, 22–33 (2015).
- 509 5. Verón, G. L. *et al.* Impact of age, clinical conditions, and lifestyle on routine semen
510 parameters and sperm kinematics. *Fertil Steril* **110**, 68-75.e4 (2018).
- 511 6. Evenson, D. P., Djira, G., Kasperson, K. & Christianson, J. Relationships between the
512 age of 25,445 men attending infertility clinics and sperm chromatin structure assay
513 (SCSA®) defined sperm DNA and chromatin integrity. *Fertil Steril* **114**, 311–320
514 (2020).
- 515 7. Griswold, M. D. Spermatogenesis: The Commitment to Meiosis. *Physiol Rev* **96**, 1–17
516 (2016).
- 517 8. Gosden, R. G., Richardson, D. W., Brown, N. & Davidson, D. W. Structure and
518 gametogenic potential of seminiferous tubules in ageing mice. *Reproduction* **64**, 127–
519 133 (1982).
- 520 9. Wright, W. W., Fiore, C. & Zirkin, B. R. The effect of aging on the seminiferous
521 epithelium of the brown Norway rat. *J Androl* **14**, 110–7 (1993).
- 522 10. Silva, J. V. *et al.* Effects of Age and Lifelong Moderate-Intensity Exercise Training on
523 Rats' Testicular Function. *Int J Mol Sci* **23**, 11619 (2022).
- 524 11. Asadi, A., Ghahremani, R., Abdolmaleki, A. & Rajaei, F. Role of sperm apoptosis and
525 oxidative stress in male infertility: A narrative review. *International Journal of
526 Reproductive BioMedicine (IJRM)* (2021) doi:10.18502/ijrm.v19i6.9371.
- 527 12. Gunes, S., Hekim, G. N. T., Arslan, M. A. & Asci, R. Effects of aging on the male
528 reproductive system. *J Assist Reprod Genet* **33**, 441–454 (2016).
- 529 13. Bromfield, E. G. *et al.* Differential cell death decisions in the testis: evidence for an
530 exclusive window of ferroptosis in round spermatids. *MHR: Basic science of
531 reproductive medicine* **25**, 241–256 (2019).

- 532 14. Halliwell, B. & Gutteridge, J. M. C. *Free Radicals in Biology and Medicine*. (Oxford
533 University Press, 2015). doi:10.1093/acprof:oso/9780198717478.001.0001.
- 534 15. Gao, M., Monian, P., Quadri, N., Ramasamy, R. & Jiang, X. Glutaminolysis and
535 Transferrin Regulate Ferroptosis. *Mol Cell* **59**, 298–308 (2015).
- 536 16. Dixon, S. J. et al. Ferroptosis: An Iron-Dependent Form of Nonapoptotic Cell Death.
537 *Cell* **149**, 1060–1072 (2012).
- 538 17. Schneider, M. et al. Mitochondrial glutathione peroxidase 4 disruption causes male
539 infertility. *The FASEB Journal* **23**, 3233–3242 (2009).
- 540 18. Imai, H. et al. Depletion of Selenoprotein GPx4 in Spermatocytes Causes Male
541 Infertility in Mice. *Journal of Biological Chemistry* **284**, 32522–32532 (2009).
- 542 19. Friedmann Angeli, J. P. et al. Inactivation of the ferroptosis regulator Gpx4 triggers
543 acute renal failure in mice. *Nat Cell Biol* **16**, 1180–1191 (2014).
- 544 20. Agmon, E., Solon, J., Bassereau, P. & Stockwell, B. R. Modeling the effects of lipid
545 peroxidation during ferroptosis on membrane properties. *Sci Rep* **8**, 5155 (2018).
- 546 21. Muhammad, Z. Effects of dietary vitamin E on male reproductive system. *Asian Pacific
547 Journal of Reproduction* 145–150 (2017) doi:10.12980/apjr.6.20170401.
- 548 22. Zhou, X., Shi, H., Zhu, S., Wang, H. & Sun, S. Effects of vitamin E and vitamin C on
549 male infertility: a meta-analysis. *Int Urol Nephrol* **54**, 1793–1805 (2022).
- 550 23. Saito, H., Hara, K., Kitajima, S. & Tanemura, K. Effect of vitamin E deficiency on
551 spermatogenesis in mice and its similarity to aging. *Reproductive Toxicology* **98**, 225–
552 232 (2020).
- 553 24. Sen, E., Tunali, Y. & Erkan, M. Testicular development of male mice offsprings
554 exposed to acrylamide and alcohol during the gestation and lactation period. *Hum Exp
555 Toxicol* **34**, 401–414 (2015).
- 556 25. Ueta, T. et al. Glutathione Peroxidase 4 Is Required for Maturation of Photoreceptor
557 Cells. *Journal of Biological Chemistry* **287**, 7675–7682 (2012).
- 558 26. Da Ros, M., Lehtiniemi, T., Olotu, O., Meikar, O. & Kotaja, N. Enrichment of
559 Pachytene Spermatocytes and Spermatids from Mouse Testes Using Standard
560 Laboratory Equipment. *Journal of Visualized Experiments* (2019) doi:10.3791/60271.
- 561 27. Conrad, M. et al. The Nuclear Form of Phospholipid Hydroperoxide Glutathione
562 Peroxidase Is a Protein Thiol Peroxidase Contributing to Sperm Chromatin Stability.
563 *Mol Cell Biol* **25**, 7637–7644 (2005).

- 564 28. Paniagua, R., Martín, A., Nistal, M. & Amat, P. Testicular involution in elderly men:
565 comparison of histologic quantitative studies with hormone patterns. *Fertil Steril* **47**,
566 671–679 (1987).
- 567 29. Lasiene, K. et al. Age-related morphological peculiarities of human testes. *Folia
568 Morphol (Warsz)* **80**, 122–126 (2021).
- 569 30. Endo, T. et al. Multiple ageing effects on testicular/epididymal germ cells lead to
570 decreased male fertility in mice. *Commun Biol* **7**, 16 (2024).
- 571 31. Jiang, H. et al. Quantitative histological analysis and ultrastructure of the aging human
572 testis. *Int Urol Nephrol* **46**, 879–885 (2014).
- 573 32. Petersen, P. M., Seierøe, K. & Pakkenberg, B. The total number of Leydig and Sertoli
574 cells in the testes of men across various age groups – a stereological study. *J Anat* **226**,
575 175–179 (2015).
- 576 33. Xia, Y., Zhu, W.-J., Hao, S.-F., Liang, W.-B. & Li, J. Stereological analysis of age-
577 related changes of testicular peritubular cells in men. *Arch Gerontol Geriatr* **55**, 116–
578 119 (2012).
- 579 34. Barnes, C. J., Covington, B. W. & Lee, M. Effect of Aging and Dietary Restriction on
580 Rat Testicular Germ Cell Apoptosis. *J Gerontol A Biol Sci Med Sci* **54**, B199–B204
581 (1999).
- 582 35. Morales, E. et al. Effect of ageing on the proliferation and apoptosis of testicular germ
583 cells in the Syrian hamster *Mesocricetus auratus*. *Reprod Fertil Dev* **15**, 89 (2003).
- 584 36. Kajstura, J. et al. Necrotic and apoptotic myocyte cell death in the aging heart of Fischer
585 344 rats. *American Journal of Physiology-Heart and Circulatory Physiology* **271**,
586 H1215–H1228 (1996).
- 587 37. Martin, D. S. D. et al. Apoptotic Changes in the Aged Brain Are Triggered by
588 Interleukin-1 β -induced Activation of p38 and Reversed by Treatment with
589 Eicosapentaenoic Acid. *Journal of Biological Chemistry* **277**, 34239–34246 (2002).
- 590 38. Miyahara, K., Tatehana, M., Kikkawa, T. & Osumi, N. Investigating the impact of
591 paternal aging on murine sperm miRNA profiles and their potential link to autism
592 spectrum disorder. *Sci Rep* **13**, 20608 (2023).
- 593 39. Blanco-Rodríguez, J. & Martínez-García, C. Spontaneous germ cell death in the testis
594 of the adult rat takes the form of apoptosis: re-evaluation of cell types that exhibit the
595 ability to die during spermatogenesis. *Cell Prolif* **29**, 13–31 (1996).

- 596 40. Yuan, H., Li, X., Zhang, X., Kang, R. & Tang, D. Identification of ACSL4 as a
597 biomarker and contributor of ferroptosis. *Biochem Biophys Res Commun* **478**, 1338–
598 1343 (2016).
- 599 41. Oresti, G. M. et al. Differentiation-related changes in lipid classes with long-chain and
600 very long-chain polyenoic fatty acids in rat spermatogenic cells. *J Lipid Res* **51**, 2909–
601 2921 (2010).
- 602 42. Otaka, K., Hiradate, Y., Kobayashi, N., Shirakata, Y. & Tanemura, K. Distribution of
603 the sex chromosome during mouse spermatogenesis in testis tissue sections. *J Reprod
604 Dev* **61**, 375–81 (2015).
- 605 43. Martin, R. H. et al. The chromosome constitution of 1000 human spermatozoa. *Hum
606 Genet* **63**, 305–309 (1983).
- 607 44. van Kooij, R. J. & van Oost, B. A. Determination of sex ratio of spermatozoa with a
608 deoxyribonucleic acid-probe and quinacrine staining: a comparison. *Fertil Steril* **58**,
609 384–386 (1992).
- 610 45. Quinlivan, W. L. G., Preciado, K., Long, T. L. & Sullivan, H. Separation of human X
611 and Y spermatozoa by albumin gradients and Sephadex chromatography. *Fertil Steril*
612 **37**, 104–107 (1982).
- 613 46. Watkins, P. A., Maiguel, D., Jia, Z. & Pevsner, J. Evidence for 26 distinct acyl-
614 coenzyme A synthetase genes in the human genome. *J Lipid Res* **48**, 2736–2750 (2007).
- 615 47. Bhutani, K. et al. Widespread haploid-biased gene expression enables sperm-level
616 natural selection. *Science* **371**, (2021).
- 617 48. Bensoussan, K., Morales, C. R. & Hermo, L. Vitamin E Deficiency Causes Incomplete
618 Spermatogenesis and Affects the Structural Differentiation of Epithelial Cells of the
619 Epididymis in the Rat. *J Androl* **19**, 266–288 (1998).
- 620 49. Luo, S. et al. Vitamin E and GPX4 cooperatively protect treg cells from ferroptosis and
621 alleviate intestinal inflammatory damage in necrotizing enterocolitis. *Redox Biol* **75**,
622 103303 (2024).
- 623 50. Hu, Q. et al. GPX4 and vitamin E cooperatively protect hematopoietic stem and
624 progenitor cells from lipid peroxidation and ferroptosis. *Cell Death Dis* **12**, 706 (2021).
- 625 51. Round Spermatid Nucleus Injection (ROSNI). *Fertility and Sterility* **90** (2008).
- 626 52. Levine, H. et al. Temporal trends in sperm count: a systematic review and meta-
627 regression analysis. *Hum Reprod Update* **23**, 646–659 (2017).

- 628 53. Levine, H. *et al.* Temporal trends in sperm count: a systematic review and meta-
629 regression analysis of samples collected globally in the 20th and 21st centuries. *Hum*
630 *Reprod Update* **29**, 157–176 (2023).
- 631 54. Tatehana, M., Kimura, R., Mochizuki, K., Inada, H. & Osumi, N. Comprehensive
632 histochemical profiles of histone modification in male germline cells during meiosis
633 and spermiogenesis: Comparison of young and aged testes in mice. *PLoS One* **15**,
634 e0230930 (2020).
- 635
- 636

637 **Figure legends**

638 **Fig. 1: Age-related alterations in mouse testis germ cell populations**

639 **a**, Bodyweight (g) in young and aged male mice. **b**, Testis weight (mg) in young and aged
640 males. **c**, Gonadosomatic index (testis weight/bodyweight) in young and aged males. **d**,
641 Schematic showing the process of spermatogenesis, highlighting key differentiation stages,
642 undifferentiated spermatogonia (Type A Spg), differentiating spermagotogonia (Type B Spg),
643 pachytene spermatocytes (PSs), round spermatids (RSs) and Sertoli cells (SCs). **e**,
644 Representative images of seminiferous tubules from young (top row) and aged (bottom row)
645 mice, showing cells positive for Plzf (Type A Spg marker), Kit (Type B Spg marker), Scp3
646 (meiotic PSs marker), PNA (acrosome RSs marker) and Sox9 (SCs marker). Arrowheads
647 indicate Kit positive cells. Images are merged with DAPI. Scale bar, 50 μ m. **f-j**, Quantification
648 of Plzf positive Type A Spg (**f**), Kit positive Type B Spg (**g**), Scp3 positive PSs (**h**), PNA
649 positive RSs (**i**) and Sox9 positive SCs (**j**). Quantification in (**f**) is based on 20 images per
650 mouse, whereas (**g-j**) are based on 10 images per mouse, normalized to tubule circumference.
651 Data are presented as mean \pm SD. ** $P < 0.01$, *** $P < 0.001$ determined by Two-tailed Student's
652 *t*-test or Mann-Whitney U test. Sample size: $N = 6$ mice per group (young, 3-months; aged 18-
653 months). Each dot represents one mouse.

654

655 **Fig. 2: Distinct cell death decisions in pre- and post-meiotic germ cells**

656 **a**, Percentage of seminiferous tubules containing cells TUNEL+ cells relative to the total
657 number of tubules within a section. **b**, Quantification of cell death index (number of dead
658 cells/total tubules). **c**, Image of a seminiferous tubule from a young mouse, indicating the
659 peripheral area (in between the dashed and solid line) and the luminal area (within the solid
660 line) areas. **d-g'**, Representative images of tubules in young (top row) and aged (bottom row)
661 mice stained for cell death with Casp3 and TUNEL, showing Casp3+/TUNEL+ cells (closed
662 arrowheads) in the periphery (**d, d'**), tubules with both Casp3+/TUNEL+ and Casp3-/TUNEL+
663 cells (open arrowheads) in the periphery (**e, e'**), tubules with only Casp3-/TUNEL+ cells in the
664 periphery (**f, f'**) and tubules with Casp3-/TUNEL+ in both the periphery and lumen (**g, g'**).
665 Images are merged with Hoechst. Scale bar, 50 μ m. **h, i**, Quantification of Casp3+/TUNEL+
666 and Casp3-/TUNEL+ cells in (**h**) the periphery and (**i**) luminal areas, normalized to 100 tubules.
667 Data are presented as mean \pm SD in all panels, ns = not significant, ** $P < 0.01$, *** $P < 0.001$ as
668 determined by two-tailed Student's *t*-test or Mann-Whitney U test. Sample size: $N = 6$ mice
669 per group (young, 3-months; aged 18-months). Each dot represents one mouse.

670

671 **Fig. 3: Round spermatids show hallmarks of ferroptosis**

672 **a**, Schematic outlining the procedure of obtaining RNA and protein from round spermatid
673 (RS)- enriched fractions in young and aged mice using a modified density gradient method. **b**,
674 RS enrichment analysis. Fraction 4-7 consistently showed >80% enrichment, confirmed by
675 PNA (acrosomal) staining. Scale bar, 40 μ m. **c**, Simplified diagram illustrating ferroptosis,
676 which occurs in response to excessive iron-dependent lipid peroxidation mediated by Acsl4
677 and Alox15 (red box), coupled with a loss of Gpx4 antioxidant function (green box). **d**, Gpx4
678 protein localization in young (top panel) and aged (bottom panel) mice, merged with DAPI.
679 Scale bar, 40 μ m. **e**, Western blot images showing Gpx4 protein levels relative to ActB (top),
680 with quantitative analysis (bottom). **f-j**, Quantification of the mRNA levels of the *nGpx4*
681 isoform (**f**), *mGpx4* isoform (**g**), *cGpx4* isoform (**h**), *Acsl4* (**i**) and *Alox15* (**j**), in young and aged
682 RSs showing fold change relative to *ActB*. **k**, Western blot images of 4HNE levels relative to
683 Gapdh (top), with quantitative analysis (bottom). **l**, FISH analysis of RSs with either X (red,
684 open arrowhead) or Y (green, closed arrowhead) signal (left), and quantification of the Y/X
685 ratio (Y-chromosomes/X-chromosomes, young: Y/X 1.02, $n=13,303$ vs aged: Y/X: 1.11,
686 $n=13,008$, right), merged with Hoechst. Scale bar, 5 μ m. Data are presented as mean \pm SD in
687 all panels, ns = not significant, * $P<0.05$, ** $P<0.01$, *** $P<0.001$ as determined by Two-tailed
688 Student's *t*-test or Mann-Whitney U test. Sample size: $N=6$ mice per group (young, 3-months;
689 aged, 18-months). Each dot represents one mouse.

690

691 **Fig. 4: Vitamin E modulation induces or rescues age-related changes in spermatogenesis**

692 **a**, Study design, young mice were fed either a control diet (YC) or a vitamin E-deficient diet
693 (YVE-) and aged mice were fed a control (AC) or VE-supplemented diet (AVE+) for 70 days.
694 **b,c**, Representative images of tubules containing PNA positive RSs (**b**), quantified from 10
695 images per mouse (**c**), Scale bar, 5 μ m. **d**, Representative images of tubules showing
696 Casp3+/TUNEL+ (closed arrowheads) and Casp3-/TUNEL+ (open arrowheads) cells in the
697 periphery, and Casp3-/TUNEL+ cells in the lumen. Scale bar, 50 μ m. **e**, Percentage of
698 seminiferous tubules containing cells TUNEL+ cells relative to the total number of tubules
699 within a section. **f**, Quantification of cell death index (number of dead cells/total tubules). **g,h**,
700 Quantification of Casp3+/TUNEL+ cells in the peripheral area (**g**), and Casp3-/TUNEL+ in
701 the luminal area (**h**). **i**, Western blot images of Gpx4 and ActB (top) and quantitative analysis
702 (bottom). **j-n**, Quantification of the mRNA levels of the *nGpx4* isoform (**j**), *mGpx4* isoform
703 (**k**), *cGpx4* isoform (**l**), *Ascl4* (**m**) and *Alox15* (**n**) relative to *ActB*. **o**, Western blot images of

704 4HNE relative to Gapdh (top) and quantitative analysis (bottom). **p**, FISH analysis of RSs with
705 X (Red, open arrowhead) or Y (Green, closed arrowhead) signals (left), and quantification of
706 the Y/X ratio (Y chromosomes/X chromosomes, YC: 1.02, $n = 13,100$, YVE-: 1.07, $n = 13,300$,
707 AC: 1.10, $n = 13,022$, AVE+: 1.01 $n = 12,018$). Scale bar, 5 μm merged with Hoechst. Data are
708 presented as mean \pm SD in all panels. Groups that do not share a common letter are statistically
709 different as determined by ANOVA with *post-hoc* Tukey HSD or Kruskal-Wallis with *post-*
710 *hoc* Dunn's test. Sample size: $N=6$ for panels **c**, **e-i**, **o**, and **p**; $N=9$ (YC), $N=8$ (YVE-), $N=7$
711 (AC), and $N=9$ (AVE+) for panels **j-n**. Each dot represents one mouse.
712

713 **Extended data Fig. 1: Casp3+/TUNEL+ is observed in round spermatids**

714 Representative images of tubules containing Casp3+/TUNEL+ round spermatids (closed
715 arrowheads) in young (top panel) and aged (bottom panel) mice. Scale bar, 50 μm .
716

717 **Extended data Fig. 2: Vitamin E modulation induces or rescues spermatogenesis**
718 **impairment**

719 **a,b**, Bodyweight (g) of young control (YC) and VE deficient (YVE-) mice (**a**) and aged control
720 (AC) and VE supplemented (AVE+) mice (**b**). *** $P < 0.001$ = significant fixed effect of week
721 on bodyweight, n.s = non significant fixed effect of diet on bodyweight (Mixed-model). **c**,
722 Testis weight (mg) of YC, YVE-, AC, and AVE+ mice. **d**, Gonadosomatic index (testis weight
723 /bodyweight) of YC, YVE-, AC, and AVE+ mice. **e**, Representative images of seminiferous
724 tubules in YC, YVE-, AC and AVE+ mice, containing germ cells positive for Plzf (Type A
725 Spg, top row), Kit (Type B Spg, middle row), and Scp3 (meiotic PSs, bottom row). Scale bar,
726 50 μm . **f-h**, Quantification of Plzf positive Type A Spg (**f**), Kit positive Type B Spg (**g**), Scp3
727 positive PSs (**h**). Quantification in (**f**) is based on 20 images per mouse, and in (**g**) and (**h**) is
728 based on 10 images per mouse, normalized to the circumference of each tubule. **i**, A variety of
729 tubules in YC, YVE-, AC, AVE+ mice, showing heterogeneity of cell death in the peripheral
730 and luminal areas, Casp3+/TUNEL+ cells (closed arrowheads) and Casp3-/TUNEL+ (open
731 arrowheads). Scale bar, 50 μm . **j,k**, Quantification of Casp3-/TUNEL+ cells in the peripheral
732 area (**j**), and Casp3+/TUNEL+ in the luminal area (**k**). Data is presented as mean \pm SD in all
733 panels, groups that do not share a common letter are statistically different, determined by
734 ANOVA with *post-hoc* Tukey HSD or Kruskal-Wallis with *post-hoc* Dunn's test. Each dot
735 represents one mouse. Sample size: $N=9$ (YC), $N=8$ (YVE-), $N=7$ (AC), and $N=9$ (AVE+) for
736 panels **a-d**. $N=6$ for panels **f-h**, **j, k**; Each dot represents one mouse.

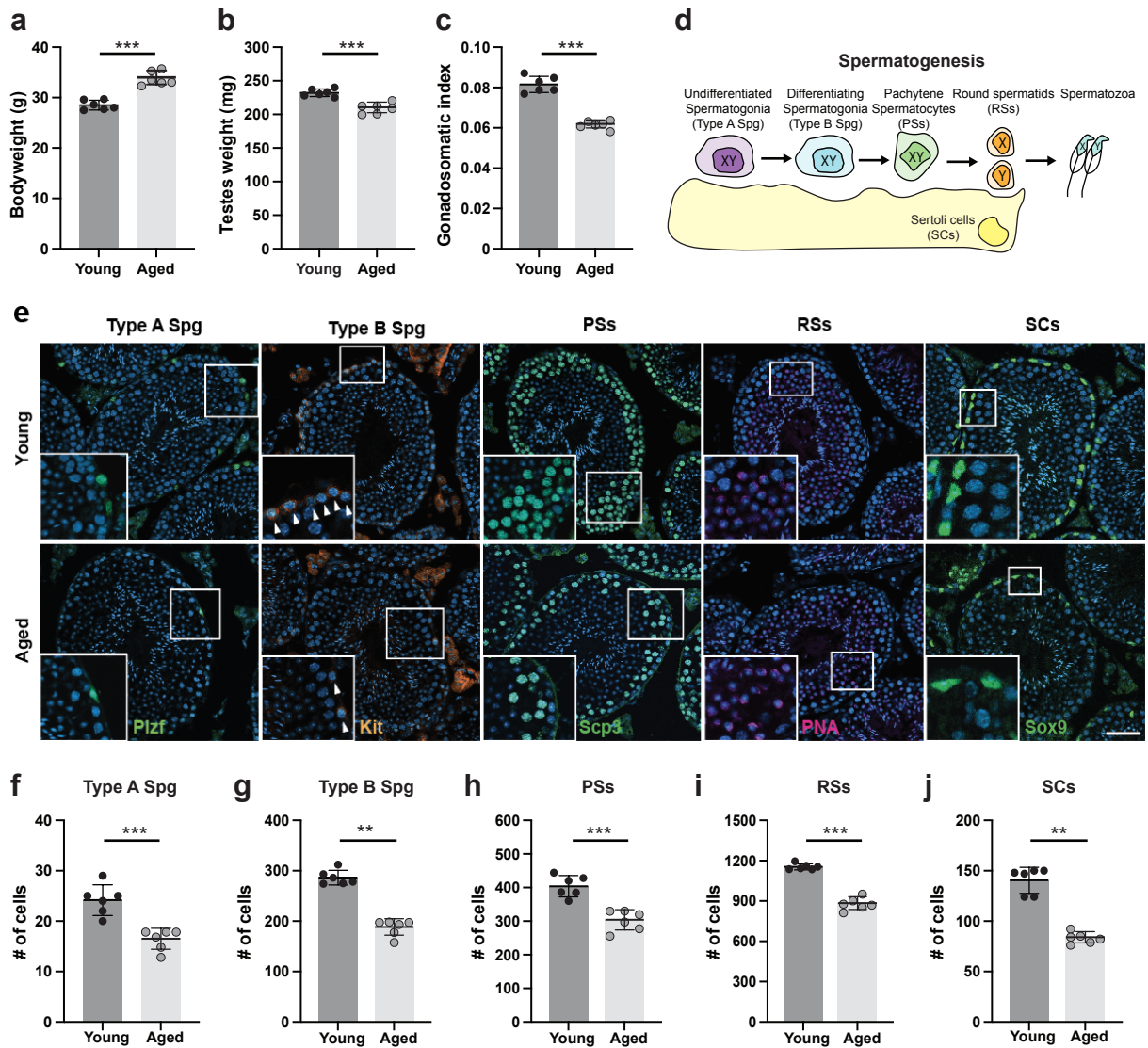


Fig. 1

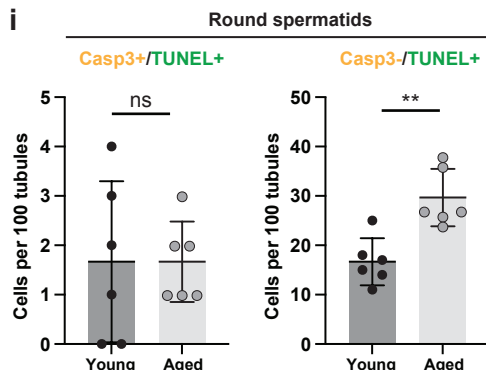
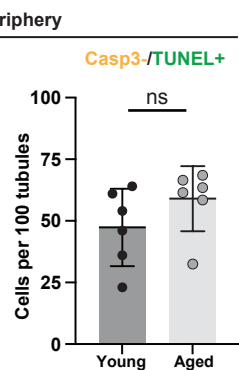
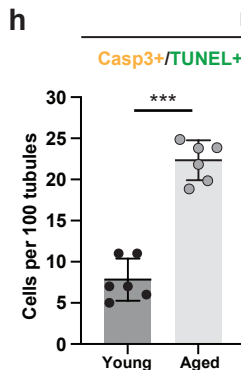
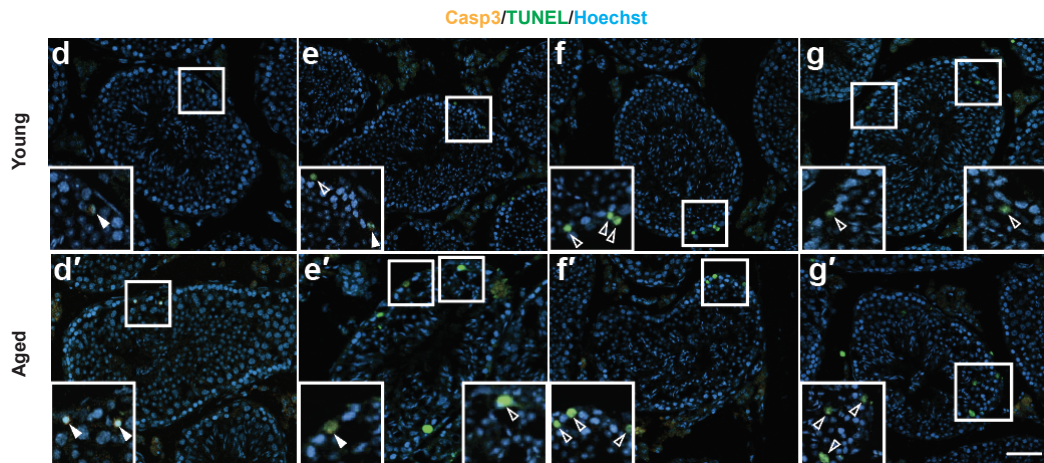
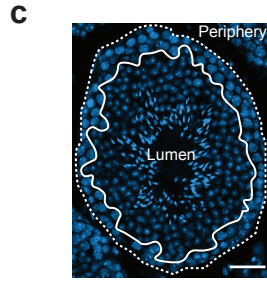
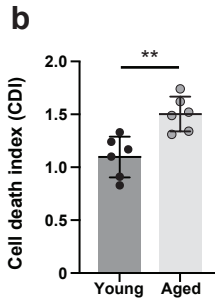
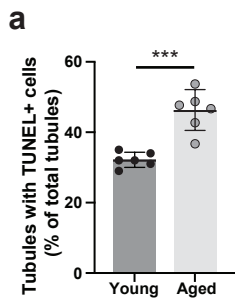


Fig. 2

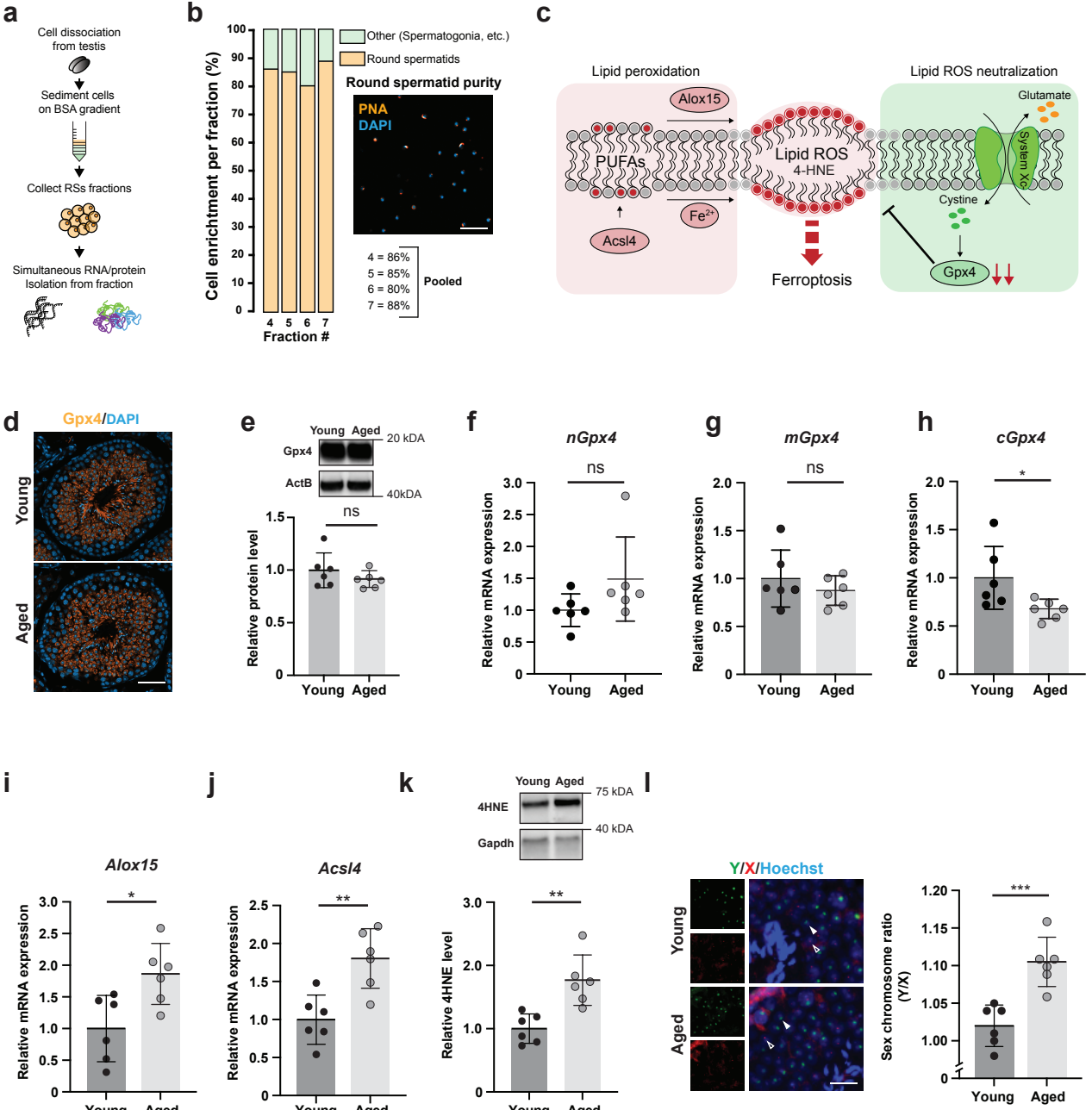


Fig. 3

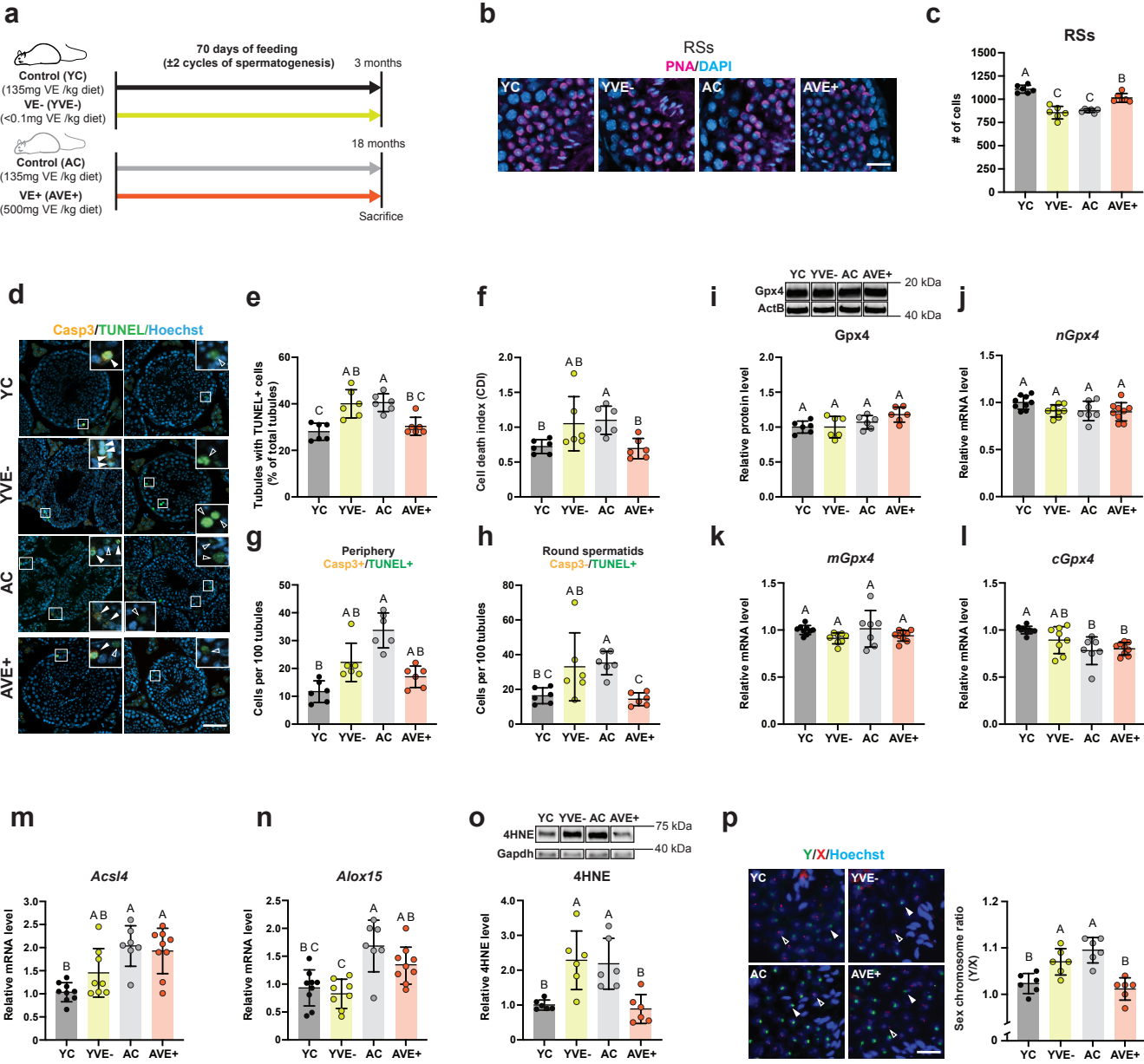
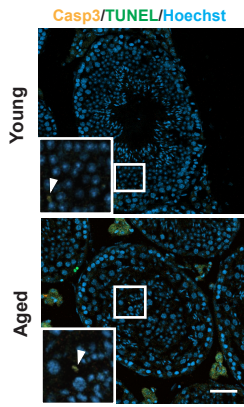
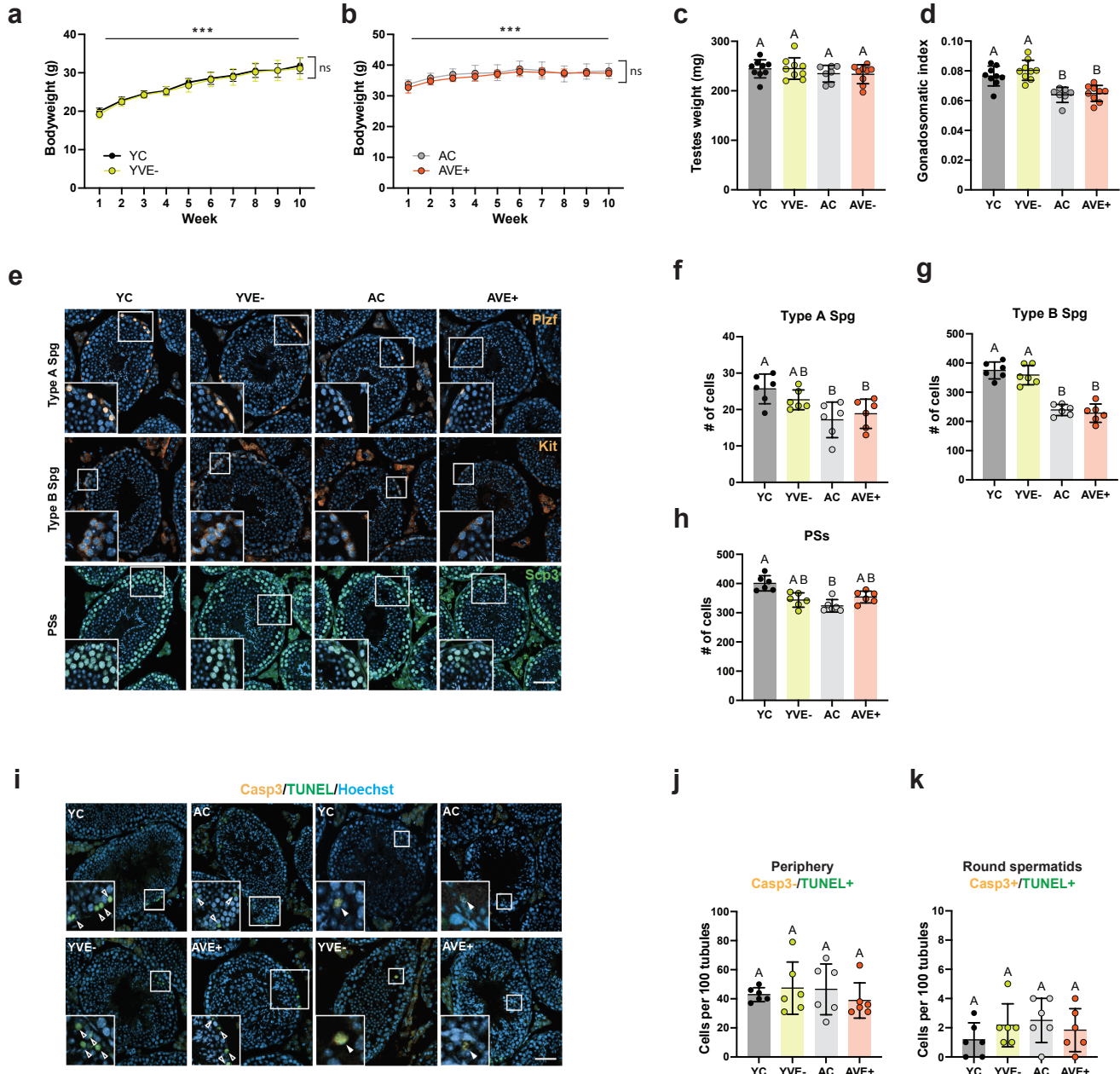


Fig. 4



Extended data Fig. 1



Extended data Fig. 2